Julia Hartl, BSc

Active site redesign of *Candida tenuis* xylose reductase to enable new reactions

Master Thesis

Institute of Biotechnology and Biochemical Engineering
Graz University of Technology

Supervisors:
Univ.-Prof. Dipl.-Ing. Dr. techn. Bernd Nidetzky
Dipl.-Ing. Dr. techn. Regina Kratzer
Dipl.-Ing. Dr. techn. Sigrid Egger

2011

EIDESSTATTLICHE ERKLÄRUNG

Ich erkläre an Eides statt, dass ich die vorliegende Arbeit selbstständig verfasst, andere als die angegebenen Quellen/Hilfsmittel nicht benutzt, und die den benutzten Quellen wörtlich und inhaltlich entnommene Stellen als solche kenntlich gemacht habe.

Graz, am …… ……..

(Unterschrift)

STATUTORY DECLARATION

I declare that I have authored this thesis independently, that I have not used other than the declared sources / resources, and that I have explicitly marked all material which has been quoted either literally or by content from the used sources.

…….. ……..

date (signature)

Acknowledgements

First, I would like to give acknowledgement to Univ.-Prof. Dipl.-Ing. Dr. techn. Bernd Nidetzky for providing me the opportunity to work at the Institute of Biotechnology and Biochemical Engineering, for his mentoring and competent advices.

I would like to express my gratitude to my supervisors Dipl.-Ing. Dr. techn. Regina Kratzer and Dipl.-Ing. Dr. techn. Sigrid Egger for their support, time and feedback throughout my work.

Thanks to the members of the Institute of Biotechnology and Biochemical Engineering for their help and assistance in the lab.

Special thanks go to my family for making all this possible and supporting me in all respects.

Last but not least I want to thank Hannes for his ongoing encouragement and patience.

Abstract

Candida tenuis xylose reductase (*Ct*XR) is a member of the mainly NAD(P)H-dependent aldo-keto reductase superfamily (AKRs) and converts xylose into xylitol, the first step of xylose metabolism in yeasts. Members of AKR subfamily 1D have evolved to reduce carbon-carbon double bonds in place of carbonyl groups. The most visible structural difference in carbon-carbon double bond reductases, as compared to carbonyl reductases, is a single active site substitution. The same replacement also enabled AKR1C9 to reduce carbon-carbon double bonds in previous studies.

In this work a set of *Ct*XR active site mutants (H113D, W23A, D50A/H113E, W23F/H113E) was designed, produced via site-directed mutagenesis and expressed in *E. coli*. The active site mutants were, after purification, screened for carbon-carbon double bond reductase activity and characterized by kinetic analysis. However, none of the active site mutants showed detectable carbon-carbon double bond reductase activity towards the utilized α,β-unsaturated carbonyl substrates, thus no alteration of chemoselectivity could be achieved. Catalytic effiencies (s^{-1} M^{-1}) for the original substrate xylose were reduced between 3000 to 8 000 000-fold as compared to the wild-type. Furthermore, the change of stereoselectivity in the reduction of ethyl 4-cyanobenzoylformate by the W23A mutant, as suggested by computer-assisted docking experiments, could not be verified in the experiment.

Keywords: *Candida tenuis* xylose reductase, aldo-keto reductase (AKR), carbon-carbon double bond reductase, structure-function relationships, docking

Kurzfassung

Candida tenuis Xylose Reduktase (*Ct*XR), ein Mitglied der vorwiegend NAD(P)H-abhängigen Aldo-Keto-Reduktasen (AKRs), katalysiert die Umwandlung von Xylose in Xylitol als ersten Schritt des Xylose-Metabolismus in Hefen.

Andere AKRs sind dazu übergegangen, C-C Doppelbindungen anstelle von Carbonylgruppen zu reduzieren (AKR1D). Hierbei ist der am besten erkennbare Unterschied zu den Carbonylreduktasen ein einfacher Austausch einer Aminosäure im aktiven Zentrum des Enzyms. Dieselbe Substitution ermöglichte in vorhergehenden Studien eine C-C Doppelbindungsreduktionsaktivität für AKR1C9.

In dieser Arbeit wurde eine Reihe von *Ct*XR-Mutanten (H113D, W23A, D50A/H113E, W23F/H113E) mit Hilfe von ortsgerichteter Mutagenese hergestellt und, nach Expression in *E. coli* und darauffolgender Reinigung, auf C-C Doppelbindungsreduktionsaktivität getestet und kinetisch charakterisiert.

Keine der Mutanten zeigte eine nachweisbare Doppelbindungsreduktionsaktivität für die verwendeten α,β-ungesättigten Carbonylsubstrate, folglich konnte keine Veränderung der Chemoselektivität erreicht werden. Die Werte für die katalytischen Effizienzen (s^{-1} M^{-1}) für das natürliche Substrat Xylose waren im Vergleich zum Wildtyp 3000- bis 8 000 000-fach erniedrigt.

Computerunterstützte Dockingversuche deuteten auf eine Änderung der Stereoselektivität für die W23A-Mutante für die Reduktion von Ethyl-4-cyanobenzoylformiat hin, die experimentell jedoch nicht bestätigt werden konnte.

Schlagwörter: *Candida tenuis* Xylose Reduktase, Aldo-Keto-Reduktase (AKRs), C-C Doppelbindungsreduktion, Struktur-Funktion-Zusammenhänge, Docking

Contents

1 Altering the chemoselectivity of *Candida tenuis* xylose reductase from carbonyl to carbon-carbon double bond reduction by rational design

1.1 Introduction

1.1.1 General features of aldo-keto reductases (AKRs)

The large protein superfamily of aldo-keto reductases (AKRs) comprises mainly NAD(P)H-dependent oxidoreductases catalyzing the reduction of carbonyl groups to alcohols on a broad substrate spectrum. The superfamily encompasses over 120 members found in both prokaryotes and eukaryotes. They can be divided into 15 families (AKR1-AKR15) that share a $(\beta/\alpha)_8$ barrel folding pattern and contain about 320 amino acids. [7] [17] AKRs exhibit high stereoselectivities and broad substrate specificities, a combination of features that is interesting for biocatalysis. Structure-function relationships of AKRs related to stereoselectivity and substrate specificity are, however, hardly understood.

1.1.2 *Candida tenuis* xylose reductase (*Ct*XR)

The enzyme xylose reductase from the yeast *Candida tenuis* (*Ct*XR; AKR2B5) exhibits a significant role in the xylose metabolism of yeasts by catalyzing the first reaction step, the NAD(P)H-dependent reduction of the open-chain free aldehyde D-xylose to xylitol (see Figure 1). [18]

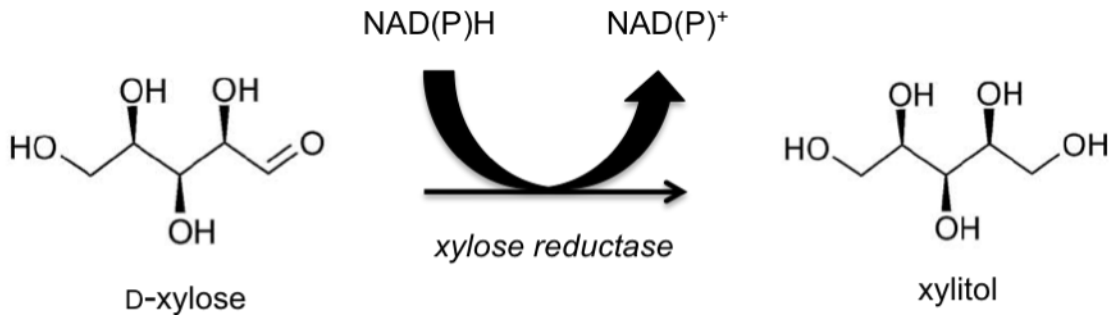

Figure 1: Conversion of D-xylose into xylitol catalyzed by NAD(P)H-dependent *Ct*XR.

AKR2B5 is a special member of the superfamily that shows distinctive features within the superfamily of AKRs. *Ct*XR forms a noncooperative homodimer composed of 36 kDa subunits [11], in contrast to the majority of AKRs that are functional monomers. Furthermore, *Ct*XR is among the rare AKRs that exhibit dual cofactor specifity; it can utilize NADH and NADPH in the reduction reaction. Previous studies have shown that the enzyme prefers the utilization of NADPH. [19]

The active site of the enzyme is composed of four catalytic residues (Asp46, Tyr51, Lys80 and His113; numbering according to *Ct*XR) [11] that support the highly stereospecific transfer of the 4-pro-*R* hydrogen of NAD(P)H to the *re*-side of the carbonyl group of the substrate [19]. This catalytic tetrad is highly conserved at the levels of primary and tertiary structure throughout the superfamily of AKRs [8]. The phenolic OH-group of Tyr51 acts as general acid/base catalyst in the reaction [1] [2] [21]. The positive charge of Lys-80 is supposed to stabilize the transition state and maintains the overall neutral charge of the active site [17]. The negatively charged Asp46 facilitates the appropriate positioning of Lys80 by formation of a salt linkage [21]. The role of His113 seems not entirely conserved in the AKRs. His113 is essential for substrate positioning in human aldose reductase [2] while catalytic assistance by optimization of the carbonyl bond charge separation and orbital alignment was assigned to His113 in *Ct*XR [13].
The reaction mechanism scheme for the reduction of carbonyl substrates is displayed in Figure 2.

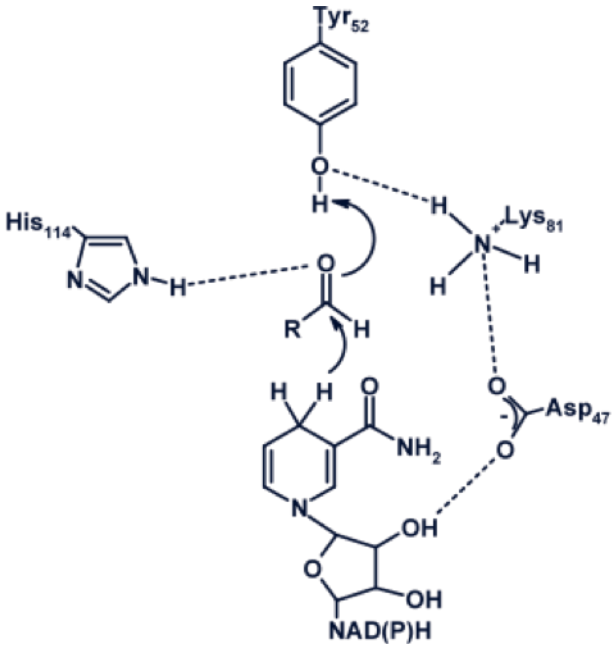

Figure 2: Reaction mechanism for the reduction of a carbonyl group with NAD(P)H-dependent *Ct*XR. The catalytic tetrad comprises the amino acids Asp46, Tyr51, Lys80 and His113.

Like other AKRs, *Ct*XR displays the common $(\beta/\alpha)_8$ barrel fold, consisting of 8 β-sheets that form the internal barrel, surrounded by 8 α-helices. The active site is built up by amino acids from several loops that connect the carboxy ends of the β-sheets to the α-helices [11].

1.1.3 Enzymatic carbon-carbon double bond reduction

Members of subfamily AKR1D have evolved to reduce carbon-carbon double bonds instead of carbonyl groups [12]. This subfamily contains the steroid 5β-reductases (Δ^4-3-ketosteroid-5β-reductases) that catalyze the reduction of Δ^4-3-ketosteroids to the corresponding 5β-reduced dihydrosteroids by reducing the carbon-carbon double bond (see Figure 3) [3] [5].

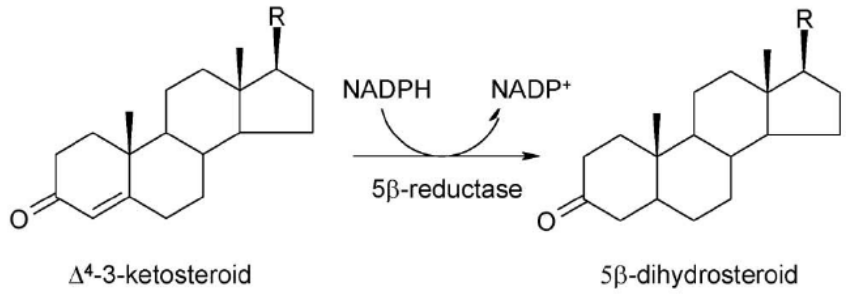

Figure 3: Reaction of 5β-reductases (AKR1D1): NADPH-dependent conversion of Δ^4-3-ketosteroid into 5β-dihydrosteroid by reduction of the C-C double bond at C-5. [17]

A multiple sequence alignment of AKRs revealed the replacement of active site histidine by glutamic acid in subfamily AKR1D. This leads to the assumption that carbon-carbon double bond reductase activity is due to a single point mutation in the catalytic tetrad [10] [15]. This hypothesis was proven by Jez and Penning (1998) who engineered 5β-reductase activity into rat liver 3α-hydroxysteroid dehydrogenase (AKR1C9) by the single active site mutation of histidine into glutamic acid [9].

1.1.4 Engineering of carbon-carbon double bond reductase activity into *Ct*XR by site-directed mutagenesis

Asymmetric carbon-carbon double bond reduction is a highly requested activity in biocatalysis and there is a growing demand for potential catalysts. The combination of C-C double bond reductase activity with the high stereoselectivity and broad substrate spectrum of *Ct*XR seems therefore promising.

Previous studies reported the replacement of His113 by glutamic acid via site-directed mutagenesis. However, no carbon-carbon double bond reductase activity was detectable with the utilized target substrate trans-cinnamaldehyde. The α,β-unsaturated aldehyde was solely converted into the corresponding α,β-unsaturated alcohol. [15]

A multiple sequence alignment of AKR2B5 with AKR1D1 led to a selection of promising single and double mutants of *Ct*XR with His113, Trp23 and Asp50 representing the key residues. An overlay of *Ct*XR and human liver Δ^4-3-ketosteroid-5β-reductase is shown in Figure 4.

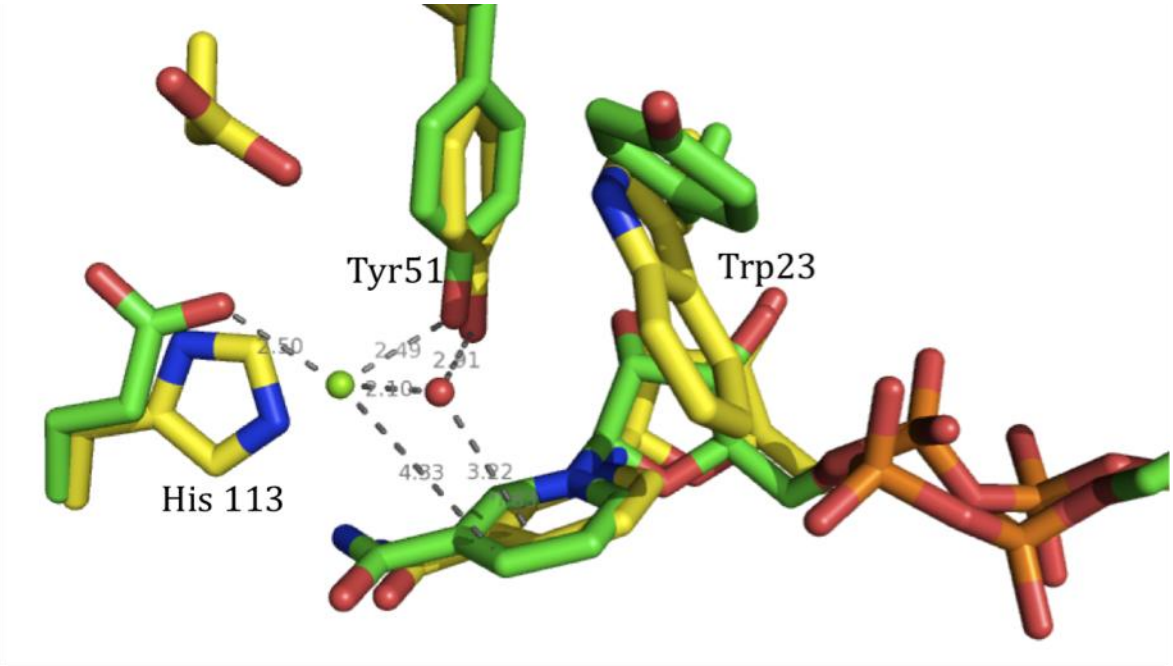

Figure 4: Overlay of AKR2B5 (yellow) with AKR1D1 (green). The steric bulk created by the residues His113 and Trp23 is removed in AKR1D1 by substitution with the smaller and more flexible side chains of glutamic acid and tyrosine respectively, thereby allowing a deeper penetration of the substrate into the binding pocket.

His113

The active site histidine takes a key role in carbonyl versus C-C double bond reductase specificity in AKRs. In the case of AKR1D1 the steric bulk of the imidazole side chain is reduced by substitution to glutamic acid. Crystallographic studies of AKR1D1 have shown that the substitution of the histidine with a glutamic acid leads to an alteration of the shape of the binding cavity due to the smaller and more flexible side chain of glutamic acid. The resulting deeper binding pocket facilitates an easier penetration of the substrate, thus allowing an appropriate positioning of the substrate in order to enable carbon-carbon double bond reduction. [6]
The aim of the mutations in *Ct*XR was to shift the β-carbon atom of α,β-unsaturated aldehydes and ketones substrate closer to the 4-pro-(*R*)-hydride of NADH. [4] Since the His→Glu mutation in *Ct*XR did not lead to the requested activity [15], various double mutants were designed. Additionally, a substitution with the even smaller side chain of aspartic acid was planned.

Trp23

The docking of xylose into the active site of *Ct*XR predicts steric conflicts of Trp23 and ketone substrates where the aldehydic proton is replaced by larger residues [11].
A multiple sequence alignment with other members of the AKR superfamily suggests an aldo versus keto discrimination by the amino acid at position 23. AKRs preferring aldehydes as substrates mostly have a tryptophan at this position, while ketone preferring AKRs often have the smaller phenylalanine or tyrosine residue there. [14]
It was previously shown that the replacement of Trp23 by Phe or Tyr led to a decrease of the aldo versus keto preference of *Ct*XR by factors of 156 and 471 respectively [14]. The results suggest that larger ketone substrates can penetrate deeper into the active site by substitution of Trp23. Therefore it was assumed that replacement of Trp23 by Ala allows for a 1,4-nucleophilic addition (reduction of carbon-carbon double bond) instead of a 1,2-nucleophilic addiction (reduction of carbonyl group) in the reduction of α,β-unsaturated carbonyls. Di Costanzo et al. have shown that the type of nucleophilic

addition is dependent on the distance between hydride and proton transfer, thus between the catalytic tyrosine and the reactive C4 hydride of NAD(P)H [5].

Asp50

A sequence comparison among AKR members has shown that most AKRs have a non-polar residue at position 50 except members of subfamily 2B. Xylose reductases display a polar aspartic acid residue at this position, located in close proximity to the catalytic tetrad. Asp50 makes a relevant contribution to the polarity of the binding pocket of xylose reductases and is furthermore substituted in AKR1D1. [11] [14]
In this work, a *Ct*XR double mutant including the substitution of aspartic acid with the non-polar side chain of alanine was planned.

1.1.5 Aim of this work

The objective of this master thesis was to engineer carbon-carbon double bond reductase activity into *Ct*XR by rational design. Based on sequence and structural alignments the following amino acids were substituted via site-directed mutagenesis:

- H113D
- W23A
- W23F/H113E
- D50A/H113E

The α,β-unsaturated aldehyde trans-cinnamaldehyde and related substances were selected as target substrates for enzymatic conversions (Figure 5). Prior to activity screening of mutants, suitable analytics of possible reduction products were set up.

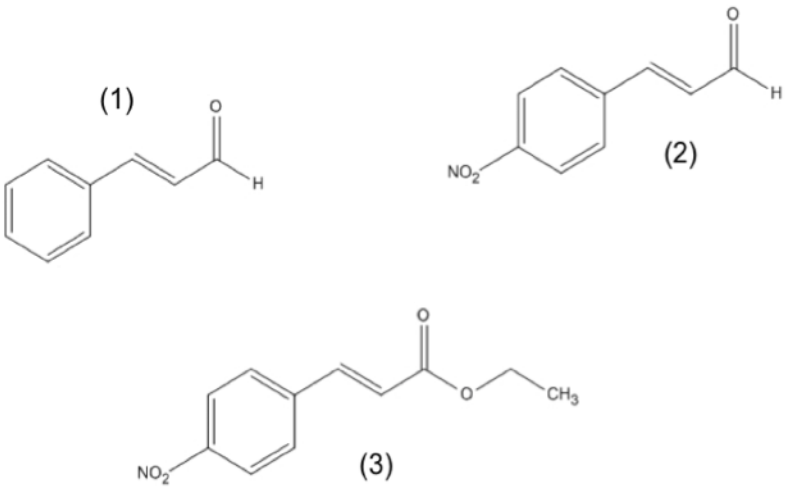

Figure 5: α,β-Unsaturated aldehyde substrates: Trans-cinnamaldehyde (1), trans-4-nitro-cinnamaldehyde (2) and ethyl 4-nitrocinnamate (3).

1.2 Materials

1.2.1 Chemicals

All chemicals used were of the highest quality and purity available. Trans-cinnamaldehyde, trans-4-nitrocinnamaldehyde, cinnamyl alcohol, ethyl 4-nitrocinnamate, hydrocinnamaldehyde and 3-phenyl-1-propanol were obtained from Sigma-Aldrich (St. Louis, USA). 3-(4-nitro-phenyl)-propionic acid ethyl ester was bought from PARAGOS (Herdecke, Germany). Strep-Tactin® Superflow® high capacity (50 % suspension) as well as D-desthiobiotin and anhydrotetracycline were purchased from IBA BioTAGnology (Göttingen, Germany). All other chemicals were either from Sigma-Aldrich/Fluka (St. Louis, USA), Roth (Karlsruhe, Germany) or Merck (Darmstadt, Germany).

1.2.2 Materials for genetic work

The pASK-IBA7plus expression plasmid was obtained from IBA BioTAGnology (Göttingen, Germany). KAPAHiFi^{TM} Hot Start PCR Kit was obtained from Peqlab (Erlangen, Germany). T4 DNA ligase and the Wizard® Plus SV Miniprep DNA Purification System were from Promega (Madison, USA). The QIAquick PCR Purification Kit and the QIAquick Gel Extraction Kit were obtained from QIAGEN (Hilden, Germany). All other enzymes as well as dNTPs and DNA standards for agarose gel electrophoresis were bought from Fermentas (St. Leon-Rot, Germany). Oligonucleotides for PCR were purchased from Integrated DNA Technologies, Inc. (Leuven, Belgium).

1.2.3 Media and buffers

- LB medium: 10 g/l peptone, 5 g/l yeast extract, 5 g/l NaCl.
- LB-Amp agar plates: 10 g/l peptone, 5 g/l yeast extract, 5 g/l NaCl, 18 g/l agar-agar, 100 µg/ml ampicillin.

- SOC medium: 20 g/l tryptone, 0.58 g/l NaCl, 5 g/l yeast extract, 2 g/l $MgCl_2$, 0.18 g/l KCl, 2.46g/l $MgSO_4$, 3.46 g/l glucose.
- 50x TAE buffer: 2 M Tris, 50 mM EDTA, 1 M acetic acid, pH 8.0.
- TE buffer: 10 mM Tris and 1 mM EDTA, pH 7.5.
- Potassium phosphate buffer (PPB): 29 mM KH_2PO_4, 21 mM K_2HPO_4, pH 7.0.
- Tris buffer: 50 mM Tris, pH 7.0.

1.3 Methods

1.3.1 Cloning of *Ct*XR and *Ct*XR_H113E into pASK-IBA7plus

The *Ct*XR gene and its H113E mutant were cloned into the pASK-IBA7plus expression plasmid (see Figure 6). The Strep-Tactin® affinity tag is fused to the N-terminus of the recombinant protein in pASK-IBA7plus and facilitates protein purification by affinity chromatography. *Eco*RI and *Bam*HI were identified as suitable restriction sites for this cloning strategy.

Features of pASK–IBA7plus

	from bp	to bp
promoter	37	72
forward primer binding site	57	76
Strep-tag	160	192
factor Xa cleavage site	193	204
multiple cloning site	205	281
reverse primer binding site	349	365
f1 origin	378	816
AmpR resistance gene	965	1825
Tet-repressor	1835	2458
Col E1 origin	2611	3199

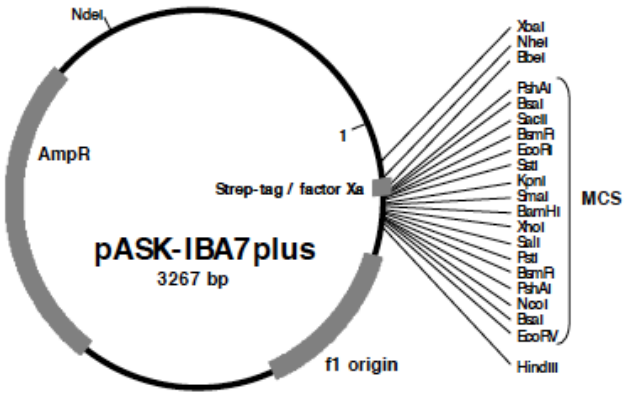

Figure 6: General features of the pASK-IBA7plus expression plasmid (IBA GmbH, Göttingen, Germany).

100 µl of a glycerol stock of *E.coli* JM109 competent cells containing the pASK-IBA7plus expression plasmid were plated onto LB-Amp agar plates. The plates were incubated at 37 °C over night. Plasmid DNA was isolated using the Wizard® Plus SV Miniprep DNA Purification System (Promega) following the protocol of the manufacturer. 50 µl of nuclease free water were used for elution of the plasmid. The purified plasmid was stored at -20 °C.

The expression plasmid was cut in a double digest using *Eco*RI and *Bam*HI restriction enzymes. The digestion mixture contained:

pASK-IBA7plus	50 µl
FastDigest® *Eco*RI	5 µl
FastDigest® *Bam*HI	5 µl
FastDigest®10x green buffer	10 µl
H_2O nuclease free	30 µl
Total volume	100 µl

The reaction mixture was incubated at 37 °C for 1-2 h with a subsequent enzyme inactivation at 80 °C for 5 min.

A preparative agarose gel with 1 % (w/v) agarose and ethidium bromide was used for visualization of the DNA fragments. Electrophoresis was carried out at 80 V for 40 min with 1x TAE as running buffer. The relevant bands were extracted out of the gel following the QIAquick Gel Extraction Kit Protocol (QIAGEN), using 40 µl nuclease free water for elution.

Dephosphorylation of the vector was carried out as follows to avoid self-ligation of the vector:

Digested pASK-IBA7plus plasmid	20 µl
Shrimp Alkaline Phosphatase	2 µl
10 x reaction buffer	3 µl
H_2O nuclease free	5 µl
Total volume	30 µl

The dephosphorylation mixture was incubated at 37 °C, after 30 min, 1 µl of Shrimp Alkaline Phosphatase was added followed by another 30 min of incubation. Inactivation of the enzyme was carried out at 65 °C for 15 min. The dephosphorylated vector was purified according to the QIAquick PCR Purification Kit Protocol (QIAGEN), using 30 µl nuclease free water for elution.

The *Ct*XR gene was amplified via PCR using the following primers with the thereby introduced restriction sites being underlined:

*Eco*RIfw: 5'- GGT CCG GAA TTC AGC GCA AGT ATC CC -3'
*Bam*HIrev: 5'- ACC CGC GGA TCC TTA AAC GAA GAT TGG -3'

Note that by utilization of the *Eco*RIfw primer, the start codon (ATG) of the gene is being removed. This is due to the consideration that it is already included in front of the strep tag.

100 µl of glycerol stocks from *E.coli* BL21 (DE3), harbouring pET11a (New England Biolabs, Ipswich, USA) with either the *Ct*XR wildtype or the H113E mutant gene on it, were plated onto LB-Amp agar plates. The plates were incubated at 37 °C over night. Plasmid DNA was isolated as described before. The eluted plasmids were used as templates in the following PCR mixture:

Template DNA	approx. 150 ng
5x KapaHifi reaction buffer	10 µl
*Eco*RIfw (10 µM)	2 µl
*Bam*HIrev (10 µM)	2 µl
Kapa dNTP Mix (10 mM)	1.5 µl
KapaHifi Hot Start Polymerase (1 U/µl)	1 µl
H_2O nuclease free	to a final volume of 50 µl

The thermal cycling profile was set up as follows:

95 °C	5 min	
98°C	20 s	
57 °C	15 s	35 cycles
72 °C	30 s	
72 °C	5 min	
4 °C	∞	

Visualization of the PCR products was done via agarose gel electrophoresis prior to purification of the PCR mixture (QIAquick PCR Purification Kit Protocol), using 50 µl nuclease free water for elution.

The amplified gene was digested with *Eco*RI and *Bam*HI restriction enzymes as follows:

Purified PCR product	50 µl
FastDigest® *Eco*Ri	3 µl
FastDigest® *Bam*HI	3 µl
FastDigest®10x green buffer	10 µl
H_2O nuclease free	7 µl
Total volume	70 µl

The reaction mixture was incubated at 37 °C for 1-2 h with a subsequent enzyme inactivation at 80 °C for 5 min. Preparative agarose gel electrophoresis and DNA extraction was carried out as described before.

Ligation was carried out as follows with a ratio of vector to insert DNA of approx. 1:3:

Expression plasmid, double-digested and dephosphorylated	approx. 200 ng
Amplified *Ct*XR gene, double-digested	approx. 200 ng
Ligase 10x buffer	1 µl
T4 DNA-Ligase	1 µl
Total volume	10 µl

The following temperature program was applied:

16 °C	60 min	17 cycles
70 °C	15 s	
4 °C	∞	

The entire ligation mixture was used for electroporation into electro-competent *E.coli* Top 10 cells (MicroPulser™, program Ec2). 800 µl of SOC medium were added directly after electroporation, followed by a regeneration phase of 1-2 h at 37 °C and 300 rpm. 50 µl and upon centrifugation the rest of the cells were plated onto LB-Amp agar plates and incubated at 37 °C over night.

Screening for positive transformants was performed via colony PCR. Single colonies were streaked onto a master plate, suspended in 50 µl TE buffer and heated to a temperature of 99 °C for 5 min, thus serving as the template DNA for the subsequent PCR.

The colony PCR mixture was set up as follows:

Template DNA	6 µl
10x dream taq buffer	2 µl
*Eco*RIfw (10 µM)	2 µl
*Bam*HIrev (10 µM)	2 µl
dNTP Mix (2 mM)	2 µl
Dream Taq Polymerase	0.5 µl
H_2O nuclease free	to a final volume of 20 µl

The temperature parameters were set up as follows:

95 °C	3 min	
95°C	40 s	
55 °C	40 s	30 cycles
72 °C	1 min	
72 °C	10 min	
4 °C	∞	

Colony PCR products were visualized via agarose gel electrophoresis. Positive colonies that showed a PCR product of the expected size on the agarose gel were streaked onto a new LB-Amp agar plate and incubated at 37 °C over night. Plasmid DNA was isolated as described before and subjected to plasmid sequencing (LGC Genomics), utilizing the following sequencing primers:

pASK-IBA7fw:	5’- GAG TTA TTT TAC CAC TCC CT -3’
pASK-IBA7rev:	5’- CGC AGT AGC GGT AAA CG -3’

1.3.2 (Two-Stage) Site-directed mutagenesis of *Ct*XR_Strep and *Ct*XR_H113E_Strep

The products of the cloning strategy described before were used as templates in a two-stage site-directed mutagenesis reaction (see Figure 7) to construct the following *Ct*XR mutants: H113D, W23A, D50A/H113E and W23F/H113E.

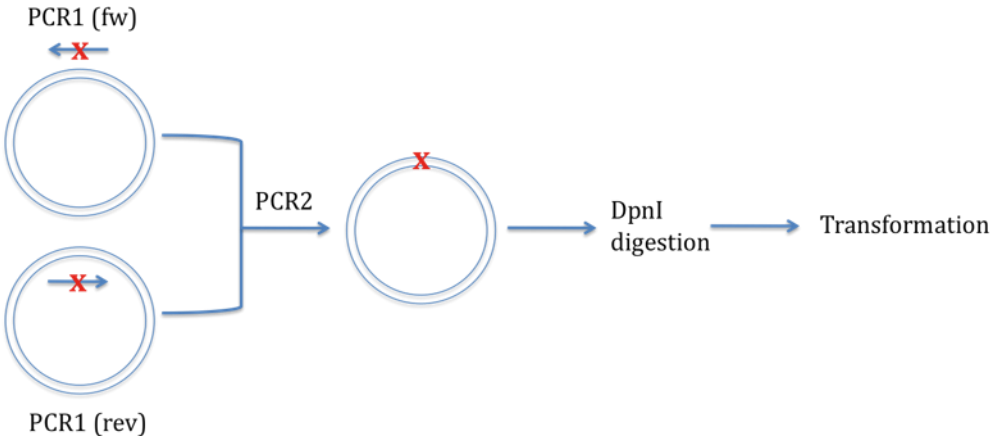

Figure 7: Two-stage PCR scheme (x = mutation)

The plasmid was directly amplified with KapaHifi Hot Start Polymerase and the oligonucleotide primers listed below (mismatched bases are underlined):

W23Afw 5'- CCATCGGTTTCGGCTGTGCGAAGCTCGCCAACGCTACC -3'
W23Arev 5'- GGTAGCGTTGGCGAGCTTCGCACAGCCGAAACCGATGG -3'
H113Dfw 5'- CGTTGACTTGTTCTTGATCGATTTCCCAATTGCCTTC -3'
H113Drev 5'- GAAGGCAATTGGGAAATCGATCAAGAACAAGTCAACG -3'

W23Ffw 5'- CCATCGGTTTCGGCTGTTTCAAGCTCGCCAACGCTACC -3'
W23Frev 5'- GGTAGCGTTGGCGAGCTTGAAACAGCCGAAACCGATGG -3'
D50Afw 5'- CGGTTACAGATTGTTCGCCGGTGCCGAGGACTACGGTAACG -3'
D50Arev 5'- CGTTACCGTAGTCCTCGGCACCGGCGAACAATCTGTAACCG -3'

The PCR mixture was set up as follows with separate reactions for forward and reverse primer:

Template DNA	approx. 3 ng
5x KapaHifi reaction buffer	5 µl
Primer fw/rev (10 µM)	1.5 µl
Kapa dNTP Mix (10 mM)	1 µl
KapaHifi Hot Start Polymerase (1 U/µl)	0.5 µl
H_2O nuclease free	to a final volume of 25 µl

The following temperature parameters were used:

95 °C	2 min	
98°C	20 s	
57 °C	15 s	4 cycles
72 °C	2.5 min	
72 °C	5 min	
4 °C	∞	

The forward and reverse reactions of each primer pair were mixed and the above mentioned temperature program was repeated, only differing in the number of cycles (20 instead of 4).

A subsequent digest with the restriction enzyme *Dpn*I was carried out to eliminate the dam-methylated template DNA. 1 µl *Dpn*I was added to 25 µL of the reaction mixture and was incubated at 37 °C for 1h. *Dpn*I digestion was repeated once to ensure full degradation of template DNA.

After visualization of the PCR products by agarose gel electrophoresis, 2 µl of the PCR product were used for electroporation into electro-competent *E. coli* Top 10 cells as described in 1.3.1.

Plasmid DNA was isolated and subjected to plasmid sequencing (LGC Genomics) to verify the introduction of the desired mutations and to exclude misincorporations.

1.3.3 Expression and purification of Strep-tagged *Ct*XR mutants

The plasmids containing the desired mutations were transformed into electro-competent *E. coli* BL 21 Star cells. Regeneration and plating onto LB-Amp agar plates was carried out as described before.

50 ml of LB medium supplemented with 100 µg/mL ampicillin were inoculated with a single colony from a LB-Amp agar plate and incubated at 37 °C and 130 rpm over night. Pre-cultures were used for inoculation of 300 mL main cultures to a target OD_{600} value of 0.1. Main cultures were incubated at 37 °C and 130 rpm. The tet promoter was induced by addition of 200 µg/L anhydrotetracycline when an OD_{600} of 0.5 to 0.6 was reached. Protein expression was carried out at 22 °C and 130 rpm over night.

The cells were harvested by centrifugation at 5000 min^{-1} and 4 °C for 35 min (Sorvall RC-5B Refrigerated Superspeed Centrifuge, FAS-10c rotor). The harvested cell pellets were resuspended in 50 mM potassium phosphate buffer pH 7.0 and stored at -20 °C.

A French Press was used for cell disruption (1500 psi, 3x) with a subsequent centrifugation step at 13,000 rpm and 4 °C for 1 h to get a cleared crude cell extract. The cell lysate was subjected to protein purification according to the manufacturer's protocol (Expression and purification of proteins using *Strep*-tag and/or 6xHistidine-tag; A comprehensive manual; IBA GmbH, Göttingen, Germany), using *Strep*-Tactin® Superflow® high capacity resin with a column bed volume of 2 ml.

As a second purification strategy for the D50A/H113E mutant (due to a failed purification trial with Strep-Tactin columns, see 1.4.1), a Red31 dye-ligand column (Pharmacia Biotech) with a column bed volume of 42.47 ml was used on a ÄKTA FPLC system (Amersham Biosciences), equilibrated with 50 mM potassium phosphate buffer pH 7.0.

For elution of adsorbed protein, a step gradient of 0.2 M and 2 M NaCl at a flow rate of 2 ml/min was applied. Detection was carried out using an UV and conductivity detector. Fractions of 20 ml were collected. The fractions at a NaCl concentration of 2 M were pooled and concentrated using 20 ml Vivaspin sample concentrators (10,000 MW cut off), thereby changing the buffer to 50 mM Tris/HCl pH 7.0.

After purification, the elution fractions as well as the crude lysate were analyzed via SDS-PAGE analysis (Pharmacia Biotech PhastSystem; GE Healthcare PhastGel Gradient 8-25) and subsequent visualization by Coomassie Brilliant Blue staining. A low molecular weight standard (Amersham Biosciences) was used for protein size estimation.

Protein concentrations were determined using the BCA protein assay (Thermo Scientific, Rockford, USA). Solutions of BSA at varying concentrations were used for calibration.

1.3.4 Enzymatic conversions with *Ct*XR active site mutants

Various enzymatic conversions were carried out in 50 mM PPB pH 7.0 containing 12.5 mM NADH and the following substrates at the given concentrations with a final reaction volume of 200 µl (EtOH and DMSO were added to enhance the solubility of the substrates):

Table 1: Substrates used for enzymatic conversions

Trans-cinnamaldehyde	5 mM	5 % v/v EtOH; PPB
Trans-4-nitrocinnamaldehyde	2 mM	25 % v/v DMSO; PPB
Ethyl 4-nitrocinnamate	1 mM	25 % v/v DMSO; PPB

The reaction was started by adding 0.3 - 0.5 mg/ml of the enzyme. Since the purification of the *Ct*XR D50A/H113E mutant failed (see 1.4.1), the crude extract was used for enzymatic conversions in this case.

All conversions were carried out at 25 °C and 300 rpm for approx. 24 h.

The same reaction mixtures but without adding the substrate or enzyme respectively were used as references.

1.3.5 HPLC analysis

HPLC analysis of the enzymatic conversions was carried out on a HPLC Agilent Technologies 1200 Series system with a Daicel Chiralpak AD-RH column at a temperature of 20 °C and maximum pressure of 110 bar. Detection of the samples (10 µl injection volume) was performed using an UV detector at a wavelength of 210 nm. Acetonitrile with 0.1 % trifluoracetic acid was used as the mobile phase. Two different acetonitrile gradients at a flow rate of 0.5 ml/min were applied:

Table 2: Utilized mobile phases for HPLC analysis

	Eluent A	Eluent B
Gradient 1	5 % acetonitrile	60 % acetonitrile
Gradient 2	5 % acetonitrile	90 % acetonitrile

Table 3: Gradient 1

t / min	
5	100 % A
60	100 % B
65	100 % A

Table 4: Gradient 2

t / min	
5	100 % A
90	100 % B
95	100 % A

The first gradient was applied for analysis of trans-cinnamaldehyde and trans-4-nitrocinnamaldehyde conversions, whereas the second gradient was used for analyzing the conversions of ethyl 4-nitrocinnamate.

10 mM standard solutions of the utilized substrates and potential conversion products in acetonitrile were used for standardization.

1.3.6 Enzyme activity assays

All kinetic studies were performed at 25 °C on a Beckmann DU800 spectrophotometer with a temperature control. Detection was carried out at 340 nm (ε_{NADH} (340 nm) = 6.22 mM^{-1} cm^{-1}), thereby monitoring the initial rates of NADH consumption.

Miscellaneous XR activity assays were performed in 50 mM PPB pH 7.0, containing 0.25 mM NADH and the following substrates at the given concentrations (EtOH and DMSO were added to enhance the solubility of the substrates):

Table 5: utilized substrates for enzyme activity assays

Xylose	700 mM	
Trans-cinnamaldehyde	10 mM	5 % v/v EtOH; PPB
Trans-4-nitrocinnamaldehyde	2 mM	25 % v/v DMSO; PPB
2-Cyclohexen-1-on	100 mM	PPB

The reaction mixtures always had a final volume of 500 µl. The measurements were started immediately after adding the enzyme (0.02-0.5 mg/ml, depending on the activity towards the respective substrate).

For determination of catalytic efficiencies (k_{cat}/K_M), initial rates were measured under conditions with varying substrate concentrations and a constant and saturating NADH concentration. For data analysis, enzyme activity (µmol min^{-1} ml^{-1}) was plotted vs.

substrate concentration (mol l^{-1}), with a slope that equals (v_{max}/K_M).

The following equation was used for calculation of k_{cat}/K_M values (M^{-1} s^{-1}):

Equation 1

$$\frac{k_{cat}}{K_M} = \frac{v_{\max}}{K_M} \times \frac{1}{c_{prot}} \times MW \times \frac{1}{60}$$

k_{cat}	turnover number (s^{-1})
K_M	Michaelis constant (mol l^{-1})
v_{max}	maximum rate (µmol min^{-1} ml^{-1})
c_{prot}	protein concentration (mg ml^{-1})
MW	molecular mass of xylose reductase (36.02 kDa)

Reference measurements were carried out using the same reaction mixtures but without adding the substrate or enzyme respectively.

1.4 Results

1.4.1 Expression and purification of Strep-tagged *Ct*XR mutants

SDS-PAGE analysis of the crude cell extract showed an over-expression band that migrated to exactly the same position as the wild-type (not shown). After the purification step, the SDS-PAGE showed a single band corresponding to a molecular mass of about 36 000 Da as it can be seen in Figure 8 to Figure 10.

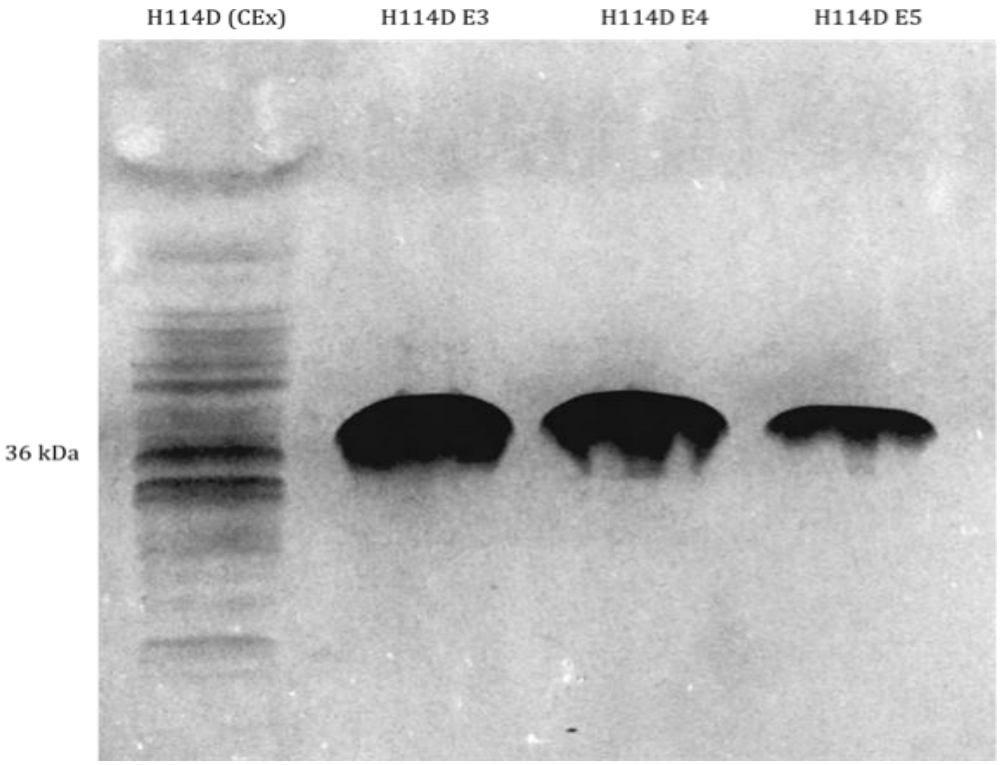

Figure 8: SDS-PAGE of H113D mutant (CEx: crude cell extract; E3-E5: elution fractions). The elution fractions show a distinct protein band at the expected size of 36 kDa.

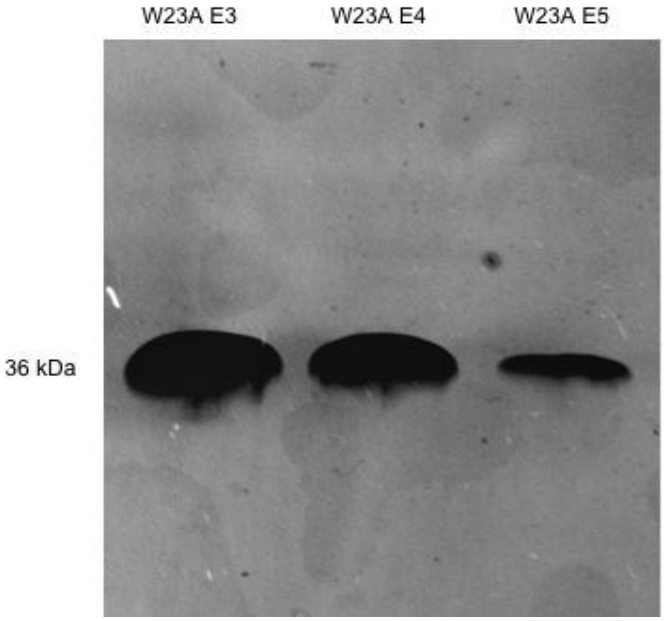

Figure 9: SDS-PAGE of W23A mutant (E3-E5: elution fractions). The elution fractions show a distinct protein band at the expected size of 36 kDa.

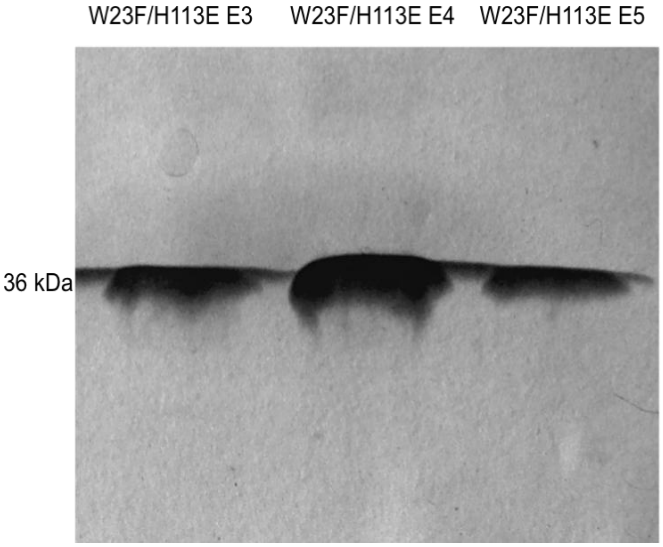

Figure 10: SDS-PAGE of W23F/H113E mutant (E3-E5: elution fractions). The elution fractions show a distinct protein band at the expected size of 36 kDa.

The D50A/H113E mutant showed a visible over-expression band on the SDS gel (Figure 11). However, it did neither bind to the Strep-Tactin nor to the Red31 dye-ligand column, thus suggesting improper folding of the enzyme.

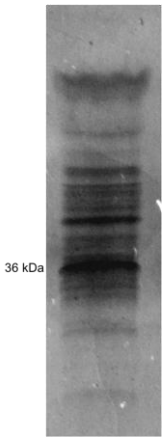

Figure 11: SDS-PAGE of *Ct*XR D50A/H113E crude cell extract with a visible over-expression band at 36 kDa.

1.4.2 Reduction of cinnamaldehyde, 4-nitrocinnamaldehyde and ethyl 4-nitrocinnamate catalyzed by *Ct*XR wild-type and active site mutants

We used chiral HPLC to analyze products from cinnamaldehyde, 4-nitrocinnamaldehyde and ethyl 4-nitrocinnamate reductions. Table 6 shows characteristic retention times of authentic standard.

Table 6: Standards used in chiral HPLC and corresponding retention times.

Standard solutions (10 mM in acetonitrile)	Retention time / min
Trans-cinnamaldehyde	46.39[1]
Cinnamyl alcohol	35.89[1]
3-Phenyl-1-propanol	33.49[1]
Hydrocinnamaldehyde	31.02[1]
	38.83[1]
Trans-4-nitrocinnamaldehyde	52.04[1]
Ethyl 4-nitrocinnamate	68.40[2]
3-(4-Nitro-phenyl)-propionic acid ethyl ester	57.84[2]

[1] gradient 1 (see Table 3)

[2] gradient 2 (see Table 4)

According to the results of HPLC analysis, the wild-type enzyme as well as all mutants converted trans-cinnamaldehyde solely into the corresponding alcohol (cinnamyl alcohol). No traces of the potential reaction products 3-phenyl-1-propanol or hydrocinnamaldehyde (see Figure 12) were detected.

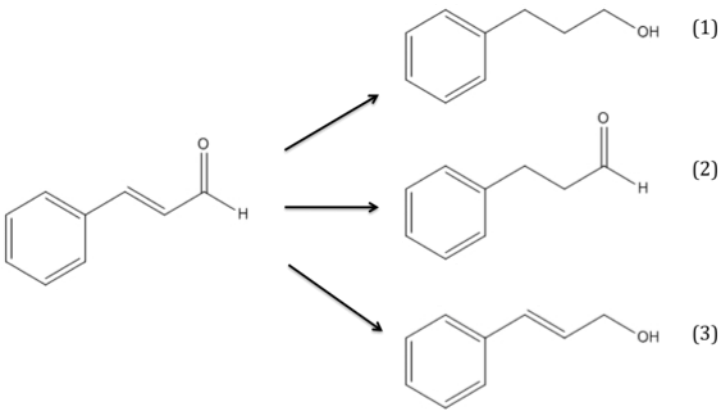

Figure 12: Potential reaction ways for the conversion of trans-cinnamaldehyde. The possible reduction products are 3-phenyl-1-propanol (1), hydrocinnamaldehyde (2) and cinnamyl alcohol (3).

In the case of trans-4-nitrocinnamaldehyde, either the single reduction product trans-4-nitrocinnamyl alcohol (wild-type, W23F/H113E and D50A/H113E) or no conversion was observed (W23A and H113D).

Conversion of the substrate ethyl 4-nitrocinnamate was neither detectable with the wild-type enzyme nor with the engineered variants.

1.4.3 Kinetic properties of *Ct*XR wild-type and active site mutants

The determined catalytic efficiencies of CtXR wild-type and the engineered active site mutants are mutants are summarized in Table 7 and

Table 8.

Table 7: Catalytic efficiencies (k_{cat}/K_M) for *Ct*XR wild-type

Substrate	(k_{cat}/K_{M}) / $(M^{-1} s^{-1})$
Xylose	136 [14]
o-Chloroacetophenone	340 [16]
Ethyl 4-cyanobenzoylformate	197 [20]
Trans-cinnamaldehyde	5740
Trans-4-nitrocinnamaldehyde	16850
2-Cyclohexen-1-on	9.174

Table 8: Catalytic efficiencies for reduction of xylose

	(k_{cat}/K_M) / $(M^{-1} s^{-1})$	Ratio WT/mutant
Wild-type	136 [14]	1
W23A	0.0494	2753
H113D	0.0000172	7 906 977
W23F/H113E	0.000457	297 593
D50A/H113E	not determined	-

1.5 Discussion

None of the *Ct*XR variants showed detectable carbon-carbon double bond reductase activity. *Ct*XR wild-type and mutants were solely capable of carbonyl group reduction. Trans-cinnamaldehyde was converted to the corresponding cinnamyl alcohol in all cases. The nitro-substituted derivative thereof and the corresponding ethyl ester have more activated carbon-carbon double bonds due to the electron-withdrawing nitro group; nonetheless the aldehyde-function was reduced to the corresponding alcohol while the C-C double bonds were not converted at all.

Enzyme activity assays of the CtXR active site mutants exhibited a dramatic loss of activity for the original activity for the original substrate xylose, in particular for those mutants with a mutation at position His113 (

position His113 (

Table 8). Our findings suggest a major impact on the general catalytic properties of the enzyme and altered substrate preferences as result of the mutations.

Summarizing, the approach of Jez and Penning (1998), where a single active site mutation led to alteration of the carbonyl versus C-C double bond chemoselectivity of 3α-hydroxysteroid dehydrogenase [9], is not applicable for *Ct*XR. Here, a more complex approach is required.

1.5.1 Conclusion

Further enzyme and/or substrate engineering seems inevitable to achieve C-C double bond reduction by *Ct*XR. In cases where rational design failed, directed evolution might lead to a C-C double bond converting enzyme. Furthermore, alternative substrates that display C-C double bonds might lead to a C-C double bond reductase based on *Ct*XR.

1.6 References

[1] Barski, O. A., Gabbay, K. H., Grimshaw, C. E., and Bohren, K. M. (1995) Mechanism of human aldehyde reductase: Characterization of the active site pocket. Biochemistry, 34, 11264-11275

[2] Bohren, K. M., Grimshaw, C. E., Lai, C.-J., Harrison, D. H., Ringe, D., Petsko, G. A., and Gabbay, K. H. (1994) Tyrosine-48 is the proton donor and histidine-110 directs substrate stereochemical selectivity in the reduction reaction of human aldose reductase: Enzyme kinetics and crystal structure of the Y48H mutant enzyme. Biochemistry, 33, 2021-2032

[3] Di Costanzo, L., Drury, J. E., Christianson, D. W., and Penning, T. M. (2009) Structure and catalytic mechanism of human steroid 5β-reductase (AKR1D1). Molecular and Cellular Endocrinology, 301, 191-198

[4] Di Costanzo, L., Drury, J. E., Penning T. M., and Christianson, D.W. (2008) Crystal structure of human liver Δ4-3-ketosteroid 5β-reductase (AKR1D1) and implications for substrate binding and catalysis. Journal of Biological Chemistry, 283, 16830-16839

[5] Di Costanzo, L., Penning, T. M., and Christianson, D. W. (2009) Aldo-keto reductases in which the conserved catalytic histidine is substituted. Chemico-Biological Interactions, 178, 127-133

[6] Faucher, F., Cantin, L., Luu-The, V., Labrie, F., and Breton, R. (2008) The crystal structure of human Δ4-3-ketosteroid 5β-reductase defines the functional role of the residues of the catalytic tetrad in the steroid double bond reduction mechanism. Biochemistry, 47, 8261-8270

[7] Hyndman, D., Bauman, D. R., Heredia, V. V., and Penning, T. M. (2003) The aldo-keto reductase superfamily homepage. Chemico-Biological Interactions, 143-144, 621-631

[8] Jez, J.M., Bennett, M. J., Schlegel, B. P., Lewis, M., and Penning, T. M. (1997) Comparative anatomy of the aldo-keto reductase superfamily. Biochemical Journal, 326, 625-636

[9] Jez, J. M., and Penning, T. M. (1998) Engineering steroid 5β-reductase activity into rat liver 3α-hydroxysteroid dehydrogenase. Biochemistry, 37, 9695-9703

[10] Jez, J.M., and Penning, T. M. (2001) The aldo-keto reductase (AKR) superfamily: An update. Chemico-Biological Interactions, 130-132, 499-525

[11] Kavanagh, K. L., Klimacek, M., Nidetzky, B., and Wilson, D. K. (2002) The structure of apo and holo forms of xylose reductase, a dimeric aldo-keto reductase from *Candida tenuis*. Biochemistry, 41, 8785-8795

[12] Kondo, K.-H., Kai, M.-H., Setoguchi, Y., Eggertsen, G., Sjöblom, P., Setoguchi, T., Okuda, K.-I., and Björkhem, I. (1994) Cloning and expression of cDNA of human Δ^4-3-oxosteroid-5-β-reductase and substrate specifity of the expressed enzyme. European Journal of Biochemistry, 219, 357-363

[13] Kratzer, R., Kavanagh, K. L., Wilson, D. K., and Nidetzky, B. (2004) Studies of the enzymic mechanism of *Candida tenuis* xylose reductase (AKR2B5): X-ray structure and catalytic reaction profile for the H113A mutant. Biochemistry, 43, 4944-4954

[14] Kratzer, R., Leitgeb, S., Wilson, D. K., and Nidetzky, B. (2006) Probing the substrate binding site of *Candida tenuis* xylose reductase (AKR2B5) with site-directed mutagenesis. Biochemical Journal, 393, 51-58

[15] Kratzer, R., and Nidetzky, B. (2005) Structure-function relationships for *Candida tenuis* xylose reductase (AKR2B5): Properties of H113E mutant. Enzymology and Molecular Biology of Carbonyl Metabolism, 12, 404-412

[16] Kratzer, R., Pukl, M., Egger, S., Vogl, M., Brecker, L., and Nidetzky, B. (2011) Enzyme identification and development of a whole-cell biotransformation for asymmetric reduction of *o*-chloroacetophenone. Biotechnology and Bioengineering, 108, 797-803

[17] Kratzer, R., Wilson, D. K., and Nidetzky, B. (2006) Critical review, catalytic mechanism and substrate selectivity of aldo-keto reductases: Insights from structure-function studies of *Candida tenuis* xylose reductase. IUBMB Life, 58(9), 499-507

[18] Lee, H. (1998) The structure and function of yeast xylose (aldose) reductases. Yeast, 14, 977-984

[19] Neuhauser, W., Haltrich, D., Kulbe, K. D., and Nidetzky, B. (1997) NAD(P)H-dependent aldose reductase from the xylose-assimilating yeast *Candida tenuis*. Isolation, characterization and biochemical properties of the enzyme. Biochemical Journal, 326, 683-692

[20] Pival, S. L., Klimacek, M., and Nidetzky, B. (2009) The catalytic mechanism of NADH-dependent reduction of 9,10-phenanthrenequinone by *Candida tenuis* xylose reductase reveals plasticity in an aldo-keto reductase active site. Biochemical Journal, 421, 43-49

[21] Schlegel, B. P., Jez, J. M., and Penning, T. M. (1998) Mutagenesis of 3 α-hydroxysteroid dehydrogenase reveals a „push-pull“ mechanism for proton transfer in aldo-keto reductases. Biochemistry, 37, 3538-3548

2 Probing the stereoselectivity of the *Candida tenuis* xylose reductase W23A mutant

2.1 Introduction

The W23A mutant of *Ct*XR was, additionally to screening for carbon-carbon double bond reductase activity, also investigated for its stereoselectivity in ketone reductions.

Generally, during a reduction reaction, the enzyme delivers the hydride either from the *si*- or the *re*-side of the ketone, thus resulting in *R*- or *S*-alcohols, respectively. The dependence of the stereochemical reaction course on the sterical requirements of the substrate is referred to as “Prelog’s rule”. [2]

*Ct*XR is a dehydrogenase with Prelog specifity; the hydride transfer occurs from the pro-*R* hydrogen to the pseudo *re*-side of the ketone (see Figure 13) [4].

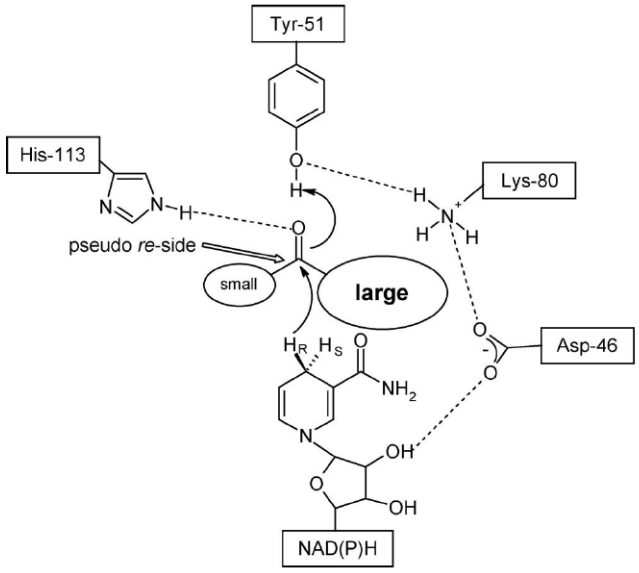

Figure 13: Mechanism for the NAD(P)H-dependent reduction of carbonyl groups with *Ct*XR. The hydride transfer occurs from the pro-*R* hydrogen to the pseudo *re*-side of the ketone. [4]

Computer-assisted docking experiments (see 2.3.5) suggested a switch in the stereoselectivity of ethyl 4-cyanobenzoylformate reduction by substitution of tryptophan with the smaller alanine at position 23.

The point mutation at position 23 (magenta) leads to a complete reorientation of the substrate ethyl 4-cyanobenzoylformate (cyan) in the binding pocket of *Ct*XR as shown in Figure 14 to Figure 17. The docking predicts that ethyl 4-cyanobenzoylformate binds in an *anti*-Prelog orientation due to removal of the steric bulk of tryptophan.

In the case of the wild-type enzyme, the ethyl residue of ethyl 4-cyanobenzoylformate points towards the aromatic indole ring system of the tryptophan while the cyano group points outwards of the binding pocket. After substitution of tryptophan by alanine, the docked ethyl 4-cyanobenzoylformate has flipped over with the ethyl group pointing outwards of the active site.

Previous reductions of ethyl 4-cyanobenzoylformate by *Ct*XR wild-type led to production of the corresponding *R*-alcohol (4-cyanomandelic acid ethyl ester) with an enantiomeric excess of 99.7 % [1]. Docking of ethyl 4-cyanobenzoylformate into the W23A mutant of *Ct*XR predicts predominant formation of the *S*-alcohol. We therefore carried out the conversion of ethyl 4-cyanobenzoylformate by W23A to test predictions of docking experiments.

Additionally, *o*-chloroacetophenone was used as a second, smaller and less bulky substrate in order to test the stereoselectivity of the W23A mutant.

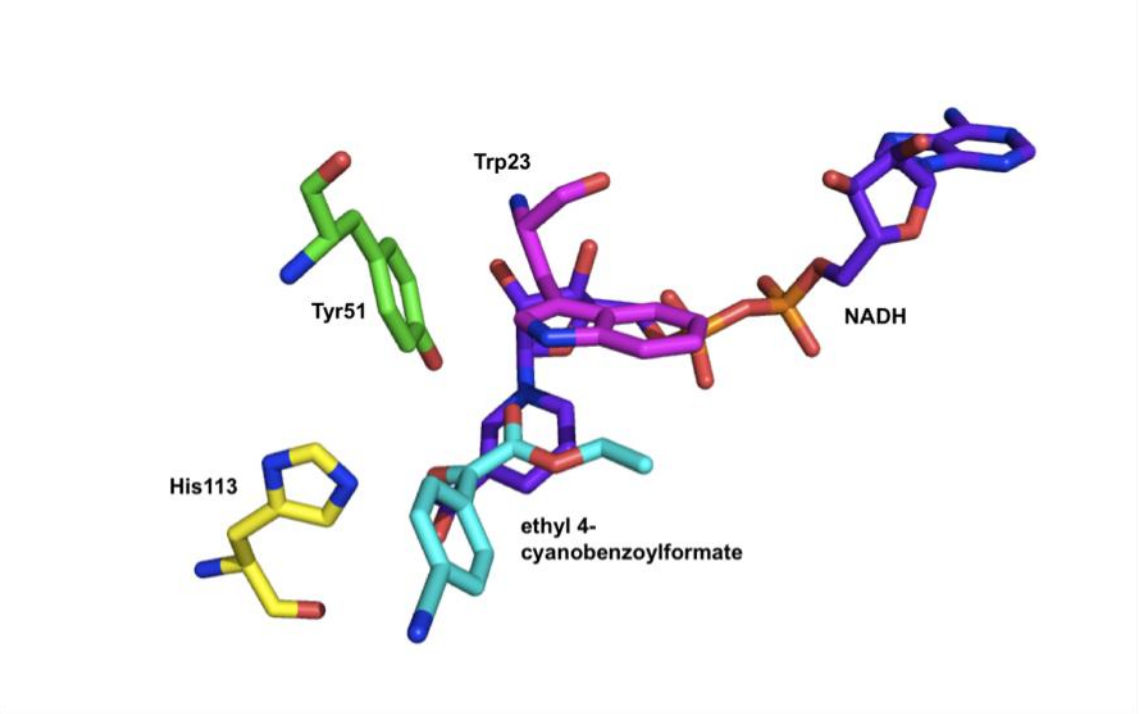

Figure 14: Docking of ethyl 4-cyanobenzoylformate into the active site of *Ct*XR wild-type (Pymol, DeLano Scientific).

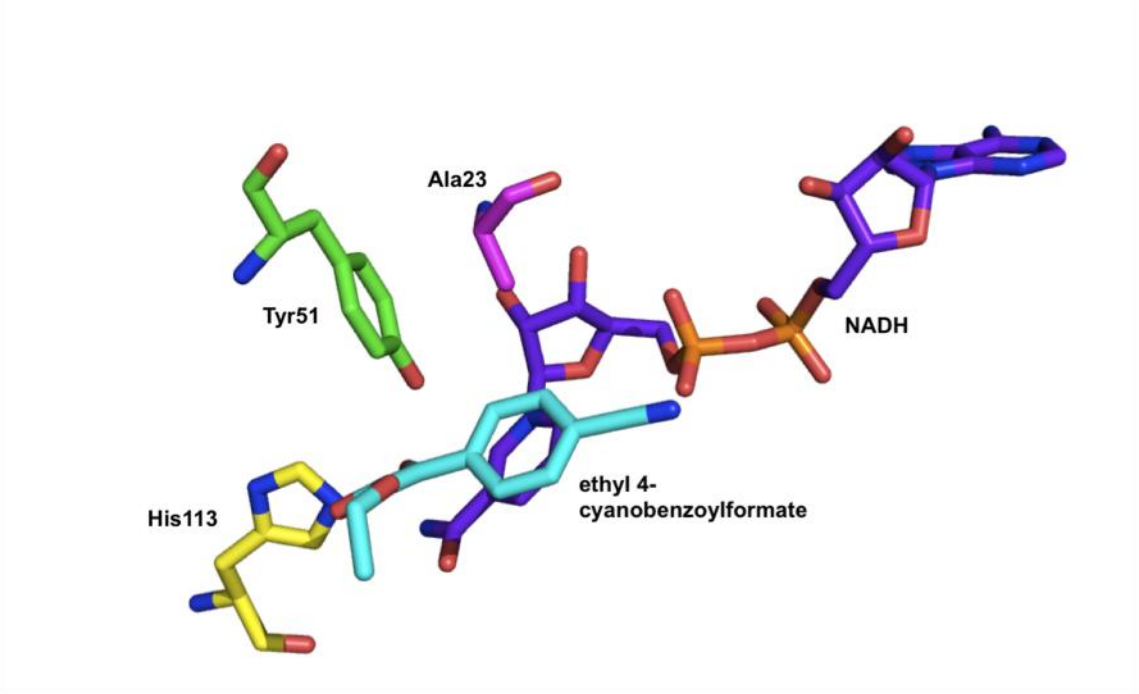

Figure 15: Docking of ethyl 4-cyanobenzoylformate into the active site of *Ct*XR W23A mutant (Pymol, DeLano Scientific).

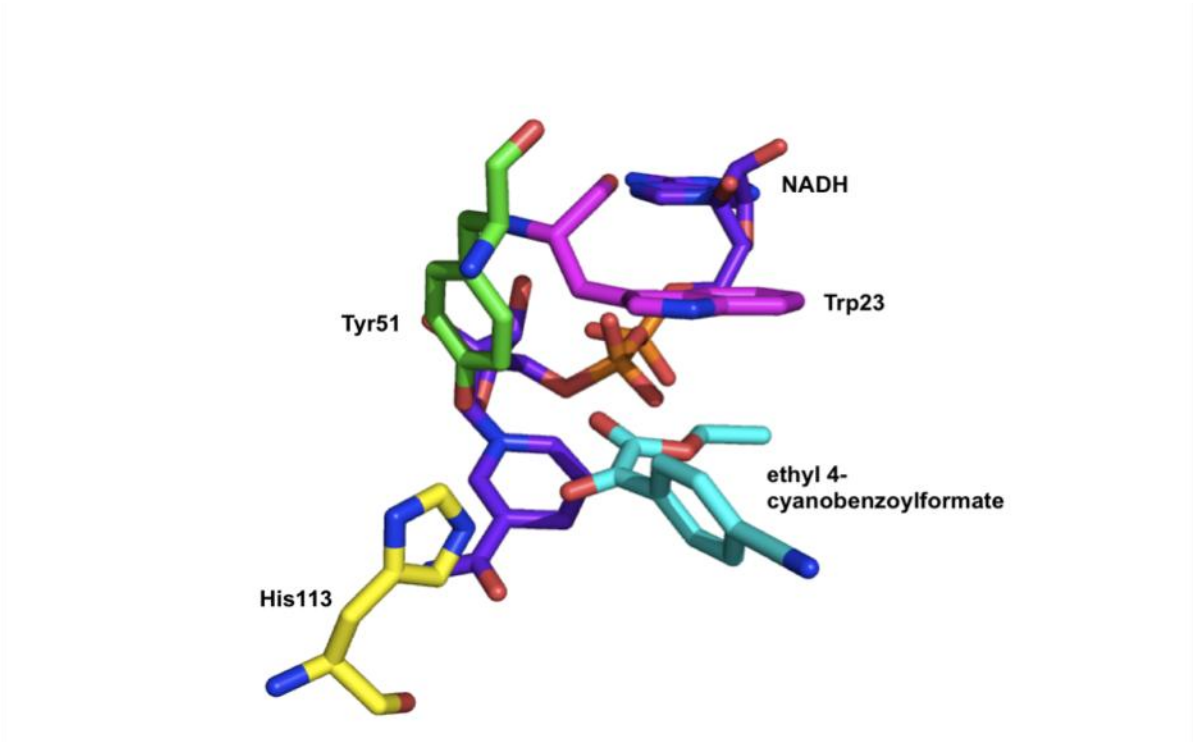

Figure 16: Docking of ethyl 4-cyanobenzoylformate into the active site of *Ct*XR wild-type (Pymol, DeLano Scientific).

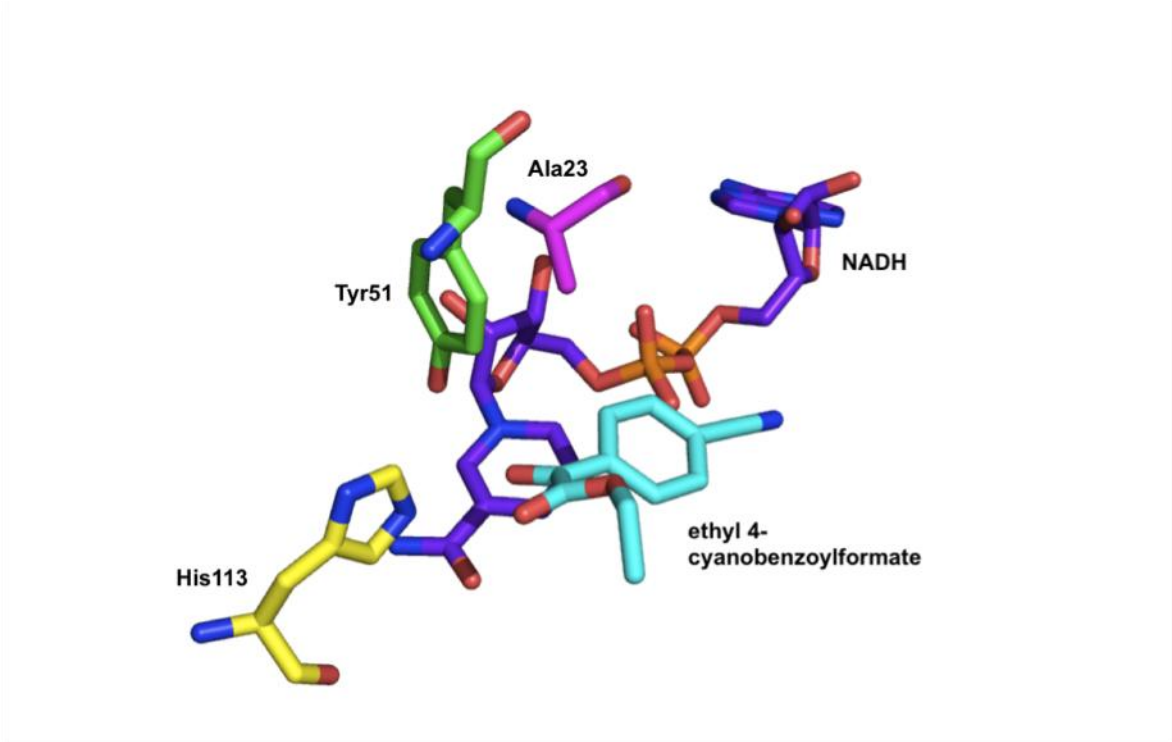

Figure 17: Docking of ethyl 4-cyanobenzoylformate into the active site of *Ct*XR W23A mutant (Pymol, DeLano Scientific).

2.2 Materials

o-Chloroacetophenone and ethyl 4-cyanobenzoylformate were obtained from Sigma-Aldrich (St. Louis, USA). 4-Cyanomandelic acid ethyl ester was bought from Synthon Chemicals GmbH & Co KG (Wolfen, Germany). 1-(2-Chlorophenyl)ethanol was from Alfa Aesar GmbH & Co KG (Karlsruhe, Germany).
All other materials used have already been described in 1.2.

2.3 Methods

2.3.1 Cloning techniques, site-directed mutagenesis, enzyme production and purification

Cloning of *Ct*XR into the pASK-IBA7plus expression plasmid was carried out as described in 1.3.1. The W23A mutant was produced using the site-directed mutagenesis method described in 1.3.2. Expression and purification of the mutant was executed according to 1.3.3.

2.3.2 Enzyme activity assays

All kinetic studies were performed at 25 °C on a Beckmann DU800 spectrophotometer equipped with a temperature control. Detection was carried out at 340 nm (ε_{NADH} (340 nm) = 6.22 mM^{-1} cm^{-1}), thereby monitoring the initial rates of NADH consumption.

*Ct*XR W23A activity assays were performed in 50 mM PPB pH 7.0, containing 0.25 mM NADH and 10 mM *o*-chloroacetophenone (5 % v/v EtOH) or 10 mM ethyl 4-cyano-benzoylformate (5 % v/v EtOH). EtOH was added to enhance the solubility of the substrates. The reaction mixtures always had a final volume of 500 µl. The

measurements were started immediately after addition of enzyme (0.02-0.5 mg/ml, depending on the activity towards the respective substrate).

Catalytic efficiencies (k_{cat}/K_M) were determined as described in 1.3.6.

Reference measurements were carried out using the same reaction mixtures but without addition of substrate or enzyme respectively.

2.3.3 Enzymatic conversions of *o*-chloroacetophenone and ethyl 4-cyanobenzoylformate

Conversions catalyzed by *Ct*XR W23A were carried out in 50 mM PPB pH 7.0, containing 12.5 mM NADH and 10 mM of the ketone-substrates listed in Table 9. Final reaction volumes were adjusted to 200 µl. EtOH was added to enhance the solubility of the substrates.

Table 9: Substrates used for enzymatic conversions

o-Chloroacetophenone	10 mM	5 % v/v EtOH; PPB
Ethyl 4-cyanobenzoylformate	10 mM	5 % v/v EtOH; PPB

The reaction was started by addition of 0.5 mg/ml enzyme. All conversions were carried out at 25 °C and 300 rpm for approx. 5 h.

2.3.4 HPLC analysis

HPLC analysis of the enzymatic conversions of *o*-chloroacetophenone and ethyl 4-cyanobenzoylformate was carried out on a HPLC Agilent Technologies 1200 Series system with a Daicel Chiralpak AD-RH column at a temperature of 40 °C and maximum pressure of 110 bar. Detection of the samples (10 µl injection volume) was performed using an UV detector at a wavelength of 210 nm.

Acetonitrile with 0.1 % trifluoracetic acid was used as the mobile phase. An isocratic method with 25 % acetonitrile was used with a run-time of 50 min.

10 mM standard solutions of the utilized substrates and racemic mixtures of the corresponding alcohols were used for standardization.

2.3.5 Docking experiments

The *Ct*XR wild-type protein crystal structure (PDB: 1mi3; 1,8 Å structure of *Ct*XR bound to NAD^+) with minimized hydrogen atoms was used for the docking experiments. Alteration of NAD^+ to NADH and protonation of His113 were carried out manually. The proton of Tyr51 was aligned. Energy minimized, induced fit docking of CtXR wild-type with ethyl 4-cyanobenzoylformate was performed using the programs Maestro and Glide (Schrödinger, LLC).
The *Ct*XR wild-type enzyme was mutated *in silico* to obtain the W23A mutant which was subsequentially structure minimized. A rigid docking of *Ct*XR W23A with ethyl 4-cyanobenzoylformate was performed.
Couture et al. proposed an optimal distance from the catalytic tyrosine residue to the carbonyl substrate of 2.47 Å, an angle of the hydride to the target carbonyl of 100.1° and a distance of the pyridine C4 to the carbonyl of 3.04 Å in AKRs [1]. The results of the docking were screened for these suggested optimal parameters. The best results are displayed in 2.1.

2.4 Results

2.4.1 Expression and purification of the Strep-tagged *Ct*XR W23A mutant

For results of protein expression and purification of *Ct*XR W23A see 1.4.1

2.4.2 HPLC analysis of enzymatic conversions of *o*-chloroacetophenone and ethyl 4-cyano-benzoylformate

Table 10 shows characteristic retention times of the utilized analytes.

Table 10: Standard solutions for HPLC analysis and their corresponding retention times

Standard solutions (10 mM in acetonitrile)	Retention time / min
o-Chloroacetophenone	36.75
4-Cyanomandelic acid ethyl ester	12.91 (*R*)
	17.33 (*S*)
1-(2-Chlorophenyl)ethanol	22.75 (*R*)
	25.69 (*S*)

According to the results of HPLC analysis, the *Ct*XR W23A mutant converted *o*-chloroacetophenone solely into the corresponding *S*-alcohol and ethyl 4-cyano-benzoylformate into the corresponding *R*-alcohol. This observation matches the results of *Ct*XR wild-type, thus no change in stereoselectivity could be observed.

2.4.3 Kinetic properties and stereoselectivities of the *Ct*XR W23A mutant

Results of kinetic measurements and HPLC analysis are summarized in Table 11 and Table 12.

Table 11: Catalytic efficiencies and stereoselectivities for reduction of *o*-chloroacetophenone

	(k_{cat}/K_M) / $(M^{-1} s^{-1})$	Ratio WT/mutant	e.e. (%)
Wild-type	340 [1]	1	> 99.9 S [1]
W23A	231	1.5	> 99.9 S

Table 12: Catalytic efficiencies and stereoselectivities for reduction of ethyl 4-cyanobenzoylformate

	(k_{cat}/K_M) / $(M^{-1} s^{-1})$	Ratio WT/mutant	e.e. (%)
Wild-type	197 [5]	1	99.7 R [5]
W23A	1525	0.13	> 99.9 R

2.5 Discussion

The *Ct*XR W23A mutant showed no change in stereoselectivity for reductions of ethyl 4-cyanobenzoylformate and *o*-chloroacetophenone as compared to the wild-type. The products ethyl *R*-4-cyanomanelate and *S*-1-(2-chlorophenyl)ethanol were obtained with enantiomeric excess values of > 99.9 %, which are similar for the wild-type reaction.

This observation is inconsistent with the results of the computer docking experiments that predicted the conversion into the ethyl *R*-4-cyanomanelate due to a reorientation of the substrate (Figure 15 and Figure 17). The contradiction between docking predictions and our result renders the informative value of docking experiments questionable. This leads to the general issue to what extent docking results are reliable.

Interestingly, the mutant showed a noticeable increase in catalytic efficiencies (k_{cat}/K_M) for ethyl 4-cyanobenzoylformate, approx. 8-fold as compared to the wild-type enzyme. This is consistent with increased catalytic efficiencies of 717 and 955 M^{-1} s^{-1} obtained with *Ct*XR W23Y and W23F variants for the reduction of ethyl 4-cyanobenzoylformate [5]. Our results confirm the assumption that substitution of the bulky tryptophan residue facilitates an easier access for larger substrates to the binding pocket.

Rates of *o*-chloroacetophenone reduction were comparable for wild-type and W23A mutant. *o*-Chloroacetophenone is a sterically less demanding molecule than ethyl 4-cyanobenzoylformate, therefore the residue at position 23 does not have a relevant impact. The methyl group points towards the side chain of Trp23 and requires only little space.

2.5.1 Conclusion

Experimental conversions of ethyl 4-cyanobenzoylformate with the *Ct*XR W23A mutant did not confirm the reaction course predicted by *in silico* docking experiments.

Apparently, the reliability of dockings can not be warranted in all cases and needs experimental approval.

2.6 References

[1] Couture, J.-F., Legrand, P., Cantin, L., van Luu-The, F.L., and Breton, R. (2004) Loop relaxation , a mechanism that explains the reduced specificity of rabbit 20α-hydroxysteroid dehydrogenase, a member of the aldo-keto reductase superfamily. Journal of Molecular Biology, 339, 89-102

[2] Faber, K. (2011) Biotransformations in organic chemistry. A textbook. Springer Berlin Heidelberg, 6th edition, 145-146

[3] Kratzer, R., Pukl, M., Egger, S., Vogl, M., Brecker, L., and Nidetzky, B. (2011) Enzyme identification and development of a whole-cell biotransformation for asymmetric reduction of *o*-chloroacetophenone. Biotechnology and Bioengineering, 108, 797-803

[4] Kratzer, R., Wilson, D. K., and Nidetzky, B. (2006) Critical review, catalytic mechanism and substrate selectivity of aldo-keto reductases: Insights from structure-function studies of *Candida tenuis* xylose reductase. IUBMB Life, 58(9), 499-507

[5] Pival, S. L., Klimacek, M., and Nidetzky, B. (2009) The catalytic mechanism of NADH-dependent reduction of 9,10-phenanthrenequinone by *Candida tenuis* xylose reductase reveals plasticity in an aldo-keto reductase active site. Biochemical Journal, 421, 43-49

3 Appendix: *Candida tenuis* xylose reductase as a potential catalyst for asymmetric reduction of imine substrates

3.1 Introduction

Imines are prochiral starting materials that allow nucleophilic attack by hydrogen or organyl groups to the carbon atom [1]. The asymmetric reduction of the C=N bond in imine substrates is a highly attractive biocatalytic reaction that facilitates the production of enantiomerically pure amines. Chiral amines are required intermediates for the production of pharmaceutical and agricultural chemicals. [1] [5] However, only few examples of biocatalytic asymmetric reduction of imines have been reported so far [5]. In addition to the main objective of this work, the C-C double bond reduction by variants of *Ct*XR, also its potential for asymmetric imine reduction has been investigated.

Figure 18 and Figure 19 show the target imine substrates, N-benzylideneaniline and phenyl-(1-phenylethylidene)amine, that were used in the present study. The first one represents an aldimine, whereas the second molecule belongs to the group of ketimines. This structural difference has a major impact on the reactivity of the substances.

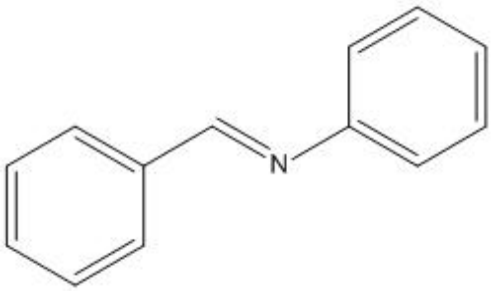

Figure 18: N-Benzylideneaniline (pK_a = 3.23)

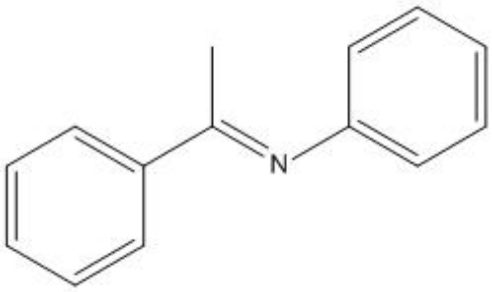

Figure 19: Phenyl-(1-phenylethylidene)amine (pK_a = 3.79)

For enzymatic conversions, the wild-type enzyme and the W23Loop mutant of *Ct*XR were used.

The W23Loop mutant contains two mutations (Trp23Phe and Lys25Ala) and subsequently three additional amino acids (Pro-Arg-Glu), which lead to the formation of a loop, thereby allowing larger substrates to slide into the active site of the enzyme [2]. This was expected to be a beneficial feature considering the size of the utilized imine substrates.

3.2 Materials

All chemicals used were of the highest quality and purity available.
N-Benzylideneaniline and phenyl-(1-phenylethylidene)amine were obtained from Sigma-Aldrich (St. Louis, USA). Deuterated dimethyl sulfoxide (DMSO-d6) and deuteriumoxide were bought from ARMAR Chemicals (Döttingen, Switzerland).
All other chemicals were either from Sigma-Aldrich/Fluka (St. Louis, USA), Roth (Karlsruhe, Germany) or Merck (Darmstadt, Germany).

3.3 Methods

3.3.1 Enzyme activity assays

All kinetic studies were performed at 25 °C on a Beckmann DU800 spectrophotometer. Detection was carried out at 340 nm (ε_{NADH} (340 nm) = 6.22 mM^{-1} cm^{-1}), thereby monitoring the initial rates of NADH consumption.

All activity assays were performed in 50 mM PPB pH 7.0, containing 0.25 mM NADH and 5 mM N-benzylideneaniline (25 % v/v DMSO) or 2 mM phenyl-(1-phenylethylidene)amine (25 % v/v DMSO). DMSO was added to enhance the solubility of the substrates. The reaction mixtures always had a final volume of 500 µl. The measurements were started immediately after addition of enzyme (0.2-0.5 mg/ml, depending on the activity towards the respective substrate).

Catalytic efficiencies (k_{cat}/K_M) were determined as described in 1.3.6.

3.3.2 Enzymatic conversion of N-benzylideneaniline

The imine substrate N-benzylideneaniline was subjected to enzymatic conversion with *Ct*XR wild-type and W23Loop mutant. Conversions were carried out in 50 mM PPB pD 6.6 in D_2O, containing 2.5 mM NADH and 2 mM N-benzylideneaniline in DMSO-d6 in a final reaction volume of 1000 µl.

The reaction was started by adding 0.5 mg/ml of the enzyme (in H_2O). All conversions were carried out at 25 °C and 300 rpm for 90 min.

3.3.3 NMR analysis

The samples of the enzymatic conversions described in 3.3.2 were subjected to NMR analysis, carried out by Prof. Hansjörg Weber at the Institute of Organic Chemistry.

^{1}H NMR spectra were recorded on a Varian INOVA-500 spectrometer with an acquisition of 32768 data points, an acquisition time of 2.048 s, a relaxation delay of 1.0 s and 64 scans. The sample temperature was 25 °C. ^{1}H irradiation and measurement frequency was 499.91 MHz. The free induction decays were directly Fourier transformed to spectra with 7998.4 Hz (^{1}H). All spectra were processed with the VNMR software. Spectra of NADH, NAD^+, aniline, benzaldehyde and benzyl alcohol were used as references.

3.4 Results

3.4.1 Kinetic properties of *Ct*XR wild-type and W23Loop mutant

The obtained kinetic parameters are summarized in Table 13 and Table 14.

Table 13: catalytic efficiencies (k_{cat}/K_M) for *Ct*XR wild-type

Substrate	$(k_{cat}/K_{M)}$ / $(M^{-1} s^{-1})$
N-Benzylideneaniline	3789
Phenyl-(1-phenylethylidene)amine	-

Table 14: catalytic efficiencies (k_{cat}/K_M) for *Ct*XR W23Loop mutant

Substrate	$(k_{cat}/K_{M)}$ / $(M^{-1} s^{-1})$
N-Benzylideneaniline	939
Phenyl-(1-phenylethylidene)amine	-

3.4.2 NMR analysis

NMR analysis of the enzymatic conversion of N-benzylideneaniline with the wild-type enzyme showed aniline and benzyl alcohol as the exclusive reaction products. Furthermore, oxidation of NADH to NAD^+ could be observed.

In the case of the *Ct*XR W23Loop mutant no NADH consumption, thus no enzymatic conversion products could be detected.

3.5 Discussion

The results of the kinetic investigations suggest that N-benzylideneaniline is converted by *Ct*XR wild-type and the W23Loop mutant. Reaction mixtures containing phenyl-(1-phenylethylidene)amine as substrate, which differs in one methyl group from N-benzylideneaniline, showed no detectable conversions.

The detected NADH consumption can be due to two possible reaction pathways, on the one hand the imine reduction, which leads to the desired amine; on the other hand a precedent hydrolysis step and a subsequent enzymatic NADH-dependent reduction of benzaldehyde to benzyl alcohol.

The reduction products of N-benzylideneaniline were assigned to aniline and benzyl alcohol by NMR analysis. These results suggest hydrolysis of N-benzylideneaniline to aniline and benzaldehyde prior to reduction of benzaldehyde to benzyl alcohol (Figure 20).

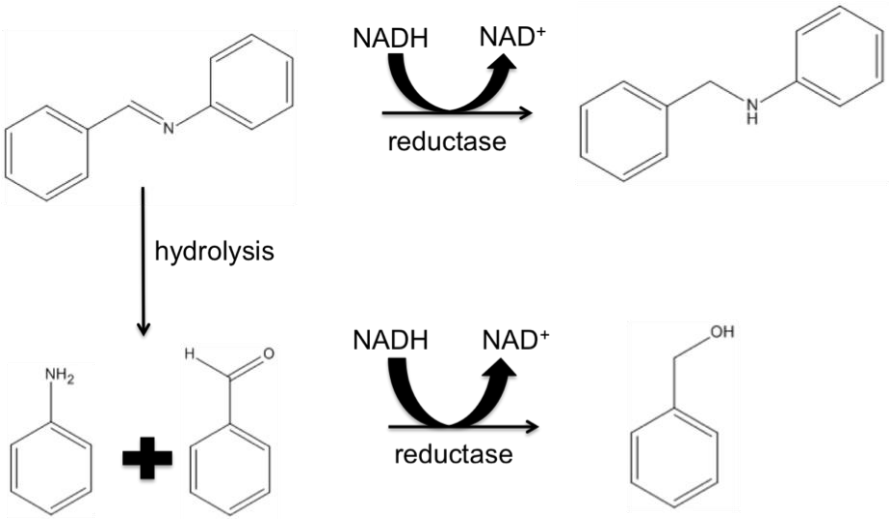

Figure 20: Potential reaction ways for N-benzylideneaniline. The two possible pathways for NADH consumption are displayed (imine reduction and hydrolysis with subsequent reduction of benzaldehyde to benzyl alcohol respectively).

This observation is consistent with the already known tendency of most imines, especially aldimines, to hydrolyze very rapidly in aqueous systems. The instability of imines represents a major problem in most asymmetric reduction approaches. [3] [5]

The fact that no catalytic efficiencies for the second substrate, phenyl-(1-phenylethylidene)amine could be determined, is also in accordance with the hydrolysis theory. The hydrolysis product of phenyl-(1-phenylethylidene)amine is acetophenone, which is no favored substrate of CtXR wild-type.

3.5.1 Conclusion

Substrate hydrolysis represents a major bottleneck in screening for imine reductase activity. Further research has to be done, particularly concerning the identification of more suitable, thus more stable substrates.

3.6 References

[1] Bräse, S., Baumann, T., Dahmen, S., and Vogt, H. (2007) Enantioselective catalytic syntheses of a-branched chiral amines. Chemical Communications, 1881-1890

[2] Krump, C. (2010) Enzymology of xylose metabolism in yeasts. Studies on wild-type and engineered forms of xylulose kinase from *Saccharomyces cerevisiae* and xylose reductase from *Candida tenuis*. II. Bachelor's Paper.

[3] Li, H., Williams, P., Micklefield, J., Gardiner, J. M., and Stephens, G. (2004) A dynamic combinatorial screen for novel imine reductase activity. Tetrahedon, 60, 753-758

[4] Mitsukura, K., Suzuki, M., Tada, K., Yoshida, T., and Nagasawa, T. (2010) Asymmetric synthesis of chiral cyclic amine from cyclic imine by bacterial whole-cell catalyst of enantioselective imine reductase. Organic and Biomolecular Chemistry, 8, 4533–4535

[5] Vaijayanth, T., and Chadha, A. (2008) Asymmetric reduction of aryl imines using *Candida parapsilosis* ATCC 7330. Tetrahedon: Asymmetry, 19, 93-96